V European Conference on Computational Fluid Dynamics
ECCOMAS CFD 2010
J. C. F. Pereira and A. Sequeira (Eds)
Lisbon, Portugal,14-17 June 2010

NUMERICAL INVESTIGATION ON THE EFFICIENCY OF A PASSIVE MICROMIXER WITH THE LATTICE BOLTZMANN METHOD

Ernesto Monaco*, Kai H. Luo† and Gunther Brenner*

*Institute for Applied Mechanics, Clausthal University,
Adolph-Roemer-Straße 2A, D-38678 Clausthal-Zellerfeld, Germany
e-mail: {ernesto.monaco, Gunther.Brenner}@tu-clausthal.de
†Energy Technology Research Group, School of Engineering Sciences,
Southampton University, SO17 1BJ Southampton, United Kingdom
e-mail: K.H.Luo@soton.ac.uk

Key words: Passive Mixing, Microfluidics, Lattice Boltzmann method.

Abstract. *A multicomponent Lattice Boltzmann scheme is employed to study the performance of a T-shaped micromixer with obstacles in its main channel. This solution was proposed in order to speed-up the mixing process which suffers because of the low-Reynolds flow regime. The two dimensional simulations conducted in this study with different flow rates and obstacle layouts demonstate the improvement of the efficiency of the mixer induced by this solution. Besides, the results show a very good agreement with a previous study in which a commercial code was adopted and provide guidelines to conveniently place the obstacles.*

1 INTRODUCTION

The mixing of two fluids is an essential process in many microfluidic devices employed in biomedical and biochemical processes like DNA purification, polymerase chain reaction (PCR), protein folding and enzyme reaction. The performance of these processes relies on rapid (order of milliseconds) and effective mixing of samples and reagen flowing in microchannels. The design of such a device has to take into account the limitations induced by the particular flow regimes occurring at microscales. Since typically $Re < 1$, microflows are laminar. Neglecting the unsteady terms, the Navier-Stokes (NS) equation reduces therefore to a balance between the pressure and the viscous term:

$$\partial_x p = \nu \partial_{yy} u. \tag{1}$$

Turbulence cannot be used to promote mixing, which instead relies on intermolecular diffusion and convection, both characterized by a specific time scale. If l is the length characterizing the mixing process, $\bar{U}$ the mean speed in the microchannel and D_{12} the mutual diffusion coefficient of the couple of fluids considered, the time scales for diffusive and convective mixing t_D and t_C, are respectively:[10,11]

$$t_D = \frac{l^2}{2D_{12}} \tag{2a}$$

$$t_C \approx \frac{l}{\bar{U}}. \tag{2b}$$

The ratio between t_C and t_D is expressed by the Peclet number Pe:

$$Pe = \frac{l\bar{U}}{D_{12}}. \tag{3}$$

Finally, the channel length L_m is given by:

$$L_m = \bar{U} \times t_D = Pe \times l \tag{4}$$

The evaluation of these quantities for real problems shows the difficulties in the design of a micromixer: diffusion in fact is a quite slow process, and the time for complete mixing in the order of milliseconds can be achieved only if l amounts to a few microns; if $l > 10\mu m$ diffusion is not efficient, because L_m would get unacceptable requiring too high pressure gradients necessary to drive the flow, with consequent problems in the design of the micropump which is present in the lab-on-a-chip device. In other words, $l \geq 100\mu m$ and $Pe > 100$ define a field of operative conditions that necessitates some form of speed up of the mixing process that does not involve a great increase of pressure drop. Micromixers are commonly classified as *active* or *passive*. Active mixing is based on the supply of external energy, while in passive mixing the flow energy due to pumping or hydrodynamic potential is used to restructure the flow in a way which results in faster

mixing. The interested reader can find a complete review of the many different solutions proposed in the last years.[12] In this study the focus will be on passive micromixers and precisely on the simplest type: the *T-shaped micromixer*. This device simply consists of two inlet channels leading two fluid streams into a main microchannel where they flow parallel. A varition is the *Y-shaped micromixer*, in which the inlets are inclined. In order to increase the mixing efficiency of such a device, in[1] it was proposed to place obstacles in the main channel of a Y-micromixer. Obstacles do not generate turbulence in the low Re flow regime characterizing the flow, but their effect is to stir the fluid creating transversal mass transport. The obstacles can be easily realized by excimer laser or silicon machining. In[1] the effect of eight different obstacle layouts on the mixing efficiency of an Y-sensor was determined by two-dimensional numerical simulations employing the commercial code MemCFD by CoventorWave ™. This approximation is acceptable when, say W and H respectively the width and the height of the main channel cross section, $W \gg H$.

In this study the Lattice Boltzmann (LB) method[2] is adopted to evaluate the efficiency of a T-mixer under different flow conditions. The LB derives from a convenient discretization of the Boltzmann equation. The algorithm is simple and suitable for massively parallel computations; incompressible NS equations are recovered with second-order accuracy. The LB is specially suited for multiphase flows in complex geometries, because it does not require special treatment to preserve interfaces and it allows a simple incorporation of curved shapes.

The rest of this paper is organized as follows: the standard LB formulation for single phase flows is introduced in the next section. Then a multiphase/multicomponent LB scheme, the Shan-Chen (SC) model is presented. This SC-LB is then validated against the results reported by Wang[1] , where circular obstacles were employed. Then the mixer performance in presence of rectangular obstacles is evaluated by different tests. Conclusions and directions for future work conclude the paper.

2 THE LATTICE BOLTZMANN METHOD

The LB method is derived from the general Boltzmann equation, which describes the evolution of the single-particle distribution function $f(\mathbf{x}, \boldsymbol{\xi}, t)$ in time because of particle streaming and collisions. This distribution function expresses the probability of finding at time t in position $\mathbf{x}$ a particle having a microscopic velocity $\boldsymbol{\xi}$. By discretizing the space $\mathbf{x}$ into a lattice $\mathcal{L}$ and the velocity space ξ into a finite set of b velocities on each lattice site, the evolution of a discrete set of particle distribution functions, $f_i(\mathbf{x}, t)$, associated with each lattice velocity $\mathbf{e}_i$ in a time step Δt is expressed by the LB equation:

$$f_i(\mathbf{x} + \mathbf{e}_i \Delta t, t + \Delta t) - f_i(\mathbf{x}, t) = -\frac{1}{\tau}\left(f_i(\mathbf{x}, t) - f_i^{eq}(\mathbf{x}, t)\right) \quad i = 1 \ldots b. \tag{5}$$

In (5), $\Delta x = |\mathbf{e}_i| \Delta t$ is the distance between two consecutive lattice sites. The streaming operator on the left hand side of equation (5) is a "shift" operation while the collision

operator is completely local. These features make the LB particularly suitable for massively parallel computations. The collision expresses the relaxation of the f_i distribution function to the local equilibrium value. The collision matrix is diagonal, with all the elements equal to the nondimensional *collision frequency* $1/\tau$. Since the *relaxation time* τ is identical for all the distribution functions, equation (5) defines the so-called single-relaxation-time LB (SRT-LB). In what follows greek indexes stay for space components, while latin ones stay for lattice directions or fluid species. The equilibrium function f_i^{eq} depends on the local macroscopic density and speed; its most general form is given by:

$$f_i^{eq} = A_i + B_i e_{i\alpha} u_\alpha + C_i u^2 + D_i e_{i\alpha} e_{i\beta} u_\alpha u_\beta + \mathcal{O}(u^3). \tag{6}$$

The constants A_i, B_i, C_i and D_i appearing in equation (6) are determined in order to recover the correct macroscopic fluid dynamics at inviscid level, that means the Euler equations. The constraints that the f_i^{eq} has to fulfill are:

$$\rho = \sum_i f_i^{eq} \tag{7a}$$

$$\rho u_\alpha = \sum_i f_i^{eq} e_{i\alpha} \tag{7b}$$

$$\Pi_{\alpha\beta}^{(0)} = \sum_i f_i^{eq} e_{i\alpha} e_{i\beta} = p\delta_{\alpha\beta} + \rho u_\alpha u_\beta. \tag{7c}$$

Equations (7a)-(7c) state that macroscopic quantities like density, momentum and energy are obtained as discrete moments of the equilibrium distribution function, while, as predicted by kinetic theory, the viscous part of the stress tensor comes from the non-equilibrium part of the f_i:

$$\Pi_{\alpha\beta}^{(1)} = \sum_i f_i^{neq} e_{i\alpha} e_{i\beta} = \sum_i (f_i - f_i^{eq}) e_{i\alpha} e_{i\beta}. \tag{8}$$

The final form of the equilibrium distribution is the following[3] :

$$f_i^{eq}(\rho, \mathbf{u}) = \rho w_i \left(1 + \frac{1}{c_s^2} e_{i\alpha} u_\alpha + \frac{1}{2c_s^4} \bar{e}_{i\alpha} \bar{e}_{i\beta} u_\alpha u_\beta\right). \tag{9}$$

where $c_s = \sqrt{RT}$ is termed the *lattice speed of sound* and is a constant depending on the lattice model, and the coefficients w_i are weighting factors that allow to build fourth-order isotropic tensors as those characterizing the NS equations even on irregular lattice models. The tensors $Q_{i\alpha\beta} = \bar{e}_{i\alpha}\bar{e}_{i\beta}$ are the traceless part of $e_{i\alpha}e_{i\beta}$ and are therefore defined as $Q_{i\alpha\beta} = e_{i\alpha}e_{i\beta} - c_s^2\delta_{\alpha\beta}$. Two of the most commonly used lattices for two-dimensional and three-dimensional simulations, respectively, are shown in figure 1, together with the components of the vectors which define them and the different w_i.

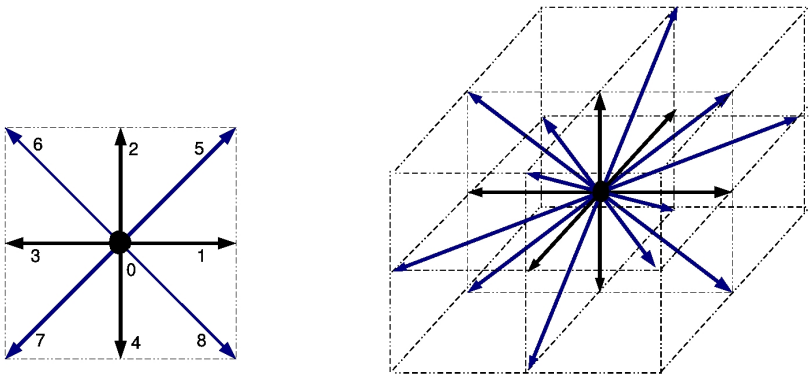

(a) (b)

Figure 1: Different lattice models for two- and three-dimensional simulations: the zero speed vector is indicated by a circle, while the slow and fast speed vectors are respectively represented by black and blue arrows. a) D2Q9; b) D3Q19

$$\mathbf{e}_i^{D2Q9} = \begin{cases} (0,0), \ w_i = 4/9, \quad i = 0, \\ (\pm 1, 0), \quad (0, \pm 1), \ w_i = 1/9, \quad i = 1 \dots 4 \\ (\pm 1, \pm 1), \ w_i = 1/36, \quad i = 5 \dots 8 \end{cases} \tag{10}$$

$$\mathbf{e}_i^{D3Q19} = \begin{cases} (0,0,0), \ w_i = 1/3, \quad i = 0, \\ (\pm 1, 0, 0), \quad (0, \pm 1, 0), \quad (0, 0, \pm 1), \ w_i = 1/18, \quad i = 1 \dots 6 \\ (\pm 1, \pm 1, 0), \quad (0, \pm 1, \pm 1), \quad (\pm 1, 0, \pm 1), \ w_i = 1/36, \quad i = 7 \dots 18 \end{cases} \tag{11}$$

The NS equations are recovered by means of a multi-scale expansion[6] . The incompressible NS are obtained with a $\mathcal{O}(Ma^3)$ term, therefore the LB is said to be a *weakly compressible method*. Thermodynamic pressure and kinematic viscosity are respectively written as:

$$p = c_s^2 \rho. \tag{12}$$

and

$$\nu = \frac{2\tau - 1}{6} \frac{\Delta x^2}{\Delta t} = \left(\tau - \frac{1}{2} \right) c_s^2 \Delta t \tag{13}$$

Pressure is therefore obtained by a state equation, rather than by solving an elliptic equation, while equation (13) prescribes that $\tau > 0.5$.

2.1 Multicomponent LB formulation: the Shan-Chen model

In a multicomponent flow different sets of f_i^j and $f_i^{j,eq}$ have to be defined for each species j, as well as different SRT "stream and collide" equations like (5):

$$f_i^j\left(\mathbf{x}+\mathbf{e}_i\Delta t, t+\Delta t\right) - f_i^j\left(\mathbf{x},t\right) = -\frac{1}{\tau^j}\left(f_i^j\left(\mathbf{x},t\right) - f_i^{j,eq}\left(\mathbf{x},t\right)\right). \tag{14}$$

In equation (14) τ^j represents the relaxation time characterizing the j-th species. In the previous section it has been shown that the standard LB formulation simulates incompressible NS with an ideal equation of state (12). In order to study multiphase/multicomponent flows nonideal effects have to be considered. The Shan-Chen[4,5] model consists in introducing a body force that mimics the interparticle interactions in order to achieve phase separation as well as non-ideal equation of state. This force is derived as gradient of a scalar potential ψ, which depends on density and it is referred to as *effective mass*. For a multicomponent flow this force takes the following expression:

$$\mathbf{F}_\alpha^j(\mathbf{x}) = -c_s^2\psi^j(\mathbf{x})\sum_i\sum_{\bar{j}} w(|\mathbf{c}|_i^2)\mathcal{G}_{j\bar{j}}\psi^{\bar{j}}(\mathbf{x}+\mathbf{c}_i)\mathbf{c}_{i\alpha}, \tag{15}$$

where $\mathcal{G}_{j\bar{j}}$ is referred to as the *coupling matrix*. It is important to underline that $\mathcal{G}_{j\bar{j}} = \mathcal{G}_{\bar{j}j}$. The interaction strength between species j and $\bar{j}$ is controlled by $\mathcal{G}_{j\bar{j}}$, which has to be positive in order to enforce separation between them. Besides, surface tension σ and diffusivity D_{12} are controlled by $\mathcal{G}$. A common choice of the effective mass for multicomponent flows is[9] $\psi^j = \rho^j$. Concerning the numerical evaluation of the gradient appearing in (14) many different finite difference schemes are possible in principle.[7] Generally speaking one has to choose a certain number N of lattice nodes $\mathbf{y}_i|\{i=1\dots N\}$ surrounding $\mathbf{x}$; say $\mathbf{c}_i = \mathbf{x}-\mathbf{y}_i|\{i=1\dots N\}$, the next step is to define a set of coefficients $w(|\mathbf{c}_i^2|)$ weighting the contributions of the different nodes, bearing in mind some constraints:

- To preserve isotropy the sites must be symmetrical about all the axis.
- Closer sites must have a bigger influence than far ones.
- The weighting factors $w(|\mathbf{c}_i^2|)$ must be chosen so to build *at least* 4-th order isotropic lattice tensors.

For each species it is possible to evaluate the momentum change produced by the corresponding force computed by equation (11) as:

$$\mathbf{u}^{j,eq} = \mathbf{u}' + \frac{\tau^j}{\rho}\mathbf{F}, \tag{16}$$

where $\mathbf{u}'$ represents an *average speed* :

$$\mathbf{u}' = \frac{\sum_j \frac{m^j}{\tau_j} \sum_i f_i^j \mathbf{e}_i}{\sum_j \frac{m^j}{\tau_j} \sum_i f_i^j}. \tag{17}$$

The total density at any lattice site is intuitively computed adding the densities of the single species. The macroscopic momentum is computed by making the average between the pre- and post-collisional states:

$$\rho u_\alpha = \sum_i f_i^j e_{i\alpha} + \frac{1}{2} \sum_j F_\alpha^j, \tag{18}$$

Finally, the kinematic viscosity and the non-ideal equation of state associated with the SC model with multiple components are given by:

$$\nu = c_s^2 \sum_j \chi^j \left(\tau^j - \frac{1}{2} \right), \tag{19a}$$

$$p = \frac{1}{3}\rho + \frac{3}{2} \sum_{j,\bar{j}} G_{j\bar{j}} \psi^j \psi^{\bar{j}} \tag{19b}$$

In equation (19a) $\chi^j = \rho^j \big/ \sum_j \rho^j$ represents the local value of the mass fraction for j-th species.

2.2 Static liquid droplet

The first case considered concerns a single static liquid droplet surrounded by another liquid. The grid is 51×51×51 and periodic boundaries are employed. D3Q19 model is adopted. The droplet has initial radius $R_i = 12$ and is placed at the centre of the domain. The initial densities inside and outside the droplet are respectively $\rho_1 = 1.1$ and $\rho_2 = 1.0$, while the coupling matrix is given by $G_{ij} = 1.0$ for $i \neq j$ and $G_{ij} = 0.0$ for $i = j$ and the relaxation times are both 1. The initial and final droplet configurations in the symmetry plane can be appreciated in figure 2a and 2b, where the concentration of component 1 is visualized. The density profile is plotted in figure 2c. The velocity field should ideally be zero everywhere; figure 2d shows instead not-negligible velocities in the interfacial region, which are referred to as *spurious currents*. This velocity field, which is produced because of the discretization of the gradient in equation (15), increase with the density ratio till they cause the simulation to blow up: their reduction is therefore crucial in order to achieve high density ratios. The maximum values of spurious currents module will be indicated here and in what follows as $|\mathbf{u}|_s$. In this particular case a value of $|\mathbf{u}|_s = 0.081$ was measured. Further tests conducted at $G_{12} = 0.1$, $G_{12} = 0.21$ and $G_{12} = 0.71$ resulted in $|\mathbf{u}|_s$ respectively equal to 0.0063, 0.01 and 0.06.

Evaluating the pressure values far from the interface and the corresponding density gradients, it is possible to determine the surface tension from Laplace's law $p_{in} - p_{out} = \frac{\sigma}{2R_f}$.

Different initial radii have been tested $(10, 12, 14, 16, 18)$, and the pressure jump has been computed, together with the final radius, for every test. As it is possible to see in figure 2d the computed points fit a straight line quite well, therefore the Laplace's law is correctly approximated.

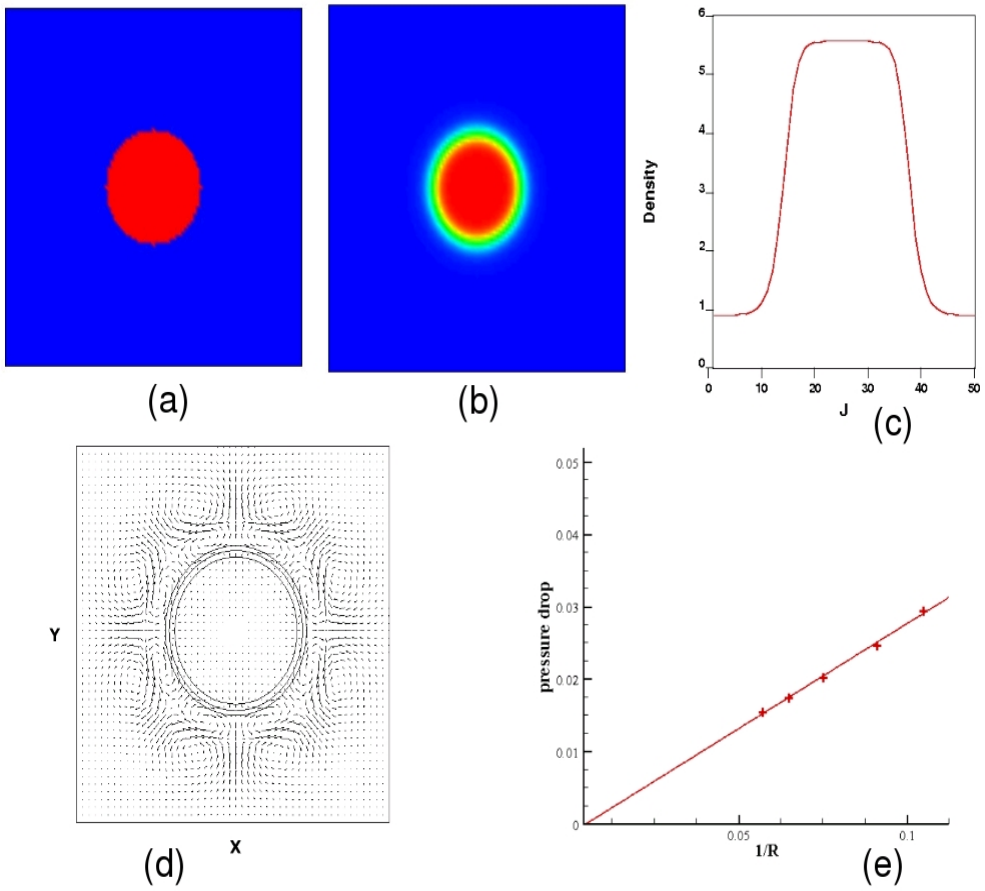

Figure 2: Static droplet case: a) Initial condition; b) Final condition; c) Density profile; d) Spurious currents; d) Verification of Laplace law. The first four pictures are related to the symmetry plane (z=25).

3 The T-shaped Micromixer

In[1] the Y-shaped micromixer was tested under different obstacle layouts. The fluids considered in[1] were water and ethanol at $Pe = 200$. Table 1 reports the main properties of these two substances. For each configuration, the mixing efficiency ε_{mix} was evaluated as in:[14]

$$\varepsilon_{mix} = \left(1 - \frac{\int_0^{2l} |\chi - \chi_\infty| dy}{\int_0^{2l} |\chi_0 - \chi_\infty| dy}\right) \times 100\%, \tag{19c}$$

where χ is the mass concentration distribution at the outflow section, χ_∞ is the concentration corresponding to a complete mixing and χ_0 is the initial concentration distribution.

Fluid	μ $(kg\,\mu m^{-1}s^{-1})$	D_{12} $(\mu m^2 s^{-1})$	ρ $(kg\,\mu m^{-3})$
Water	9.0×10^{-10}	1.2×10^{3}	9.998×10^{-16}
Ethanol	1.2×10^{-9}	1.2×10^{3}	$7.89\ \times10^{-16}$

Table 1: Properties of water and ethanol at 20° C.

Two-dimensional LB simulations were performed using the SC model for all the configurations using D2Q9 model. To have all the boundaries perfectly aligned on the grid, the T-shaped geometry was chosen: this choice was justified by what is reported in[13] , where it was demonstrated that the inclination of the inlets has not a significant effect on the mixing performance. The T-sensor is represented in figure 3, in which one of the circular obstacle layouts fabricated and tested in[1] is also reported.

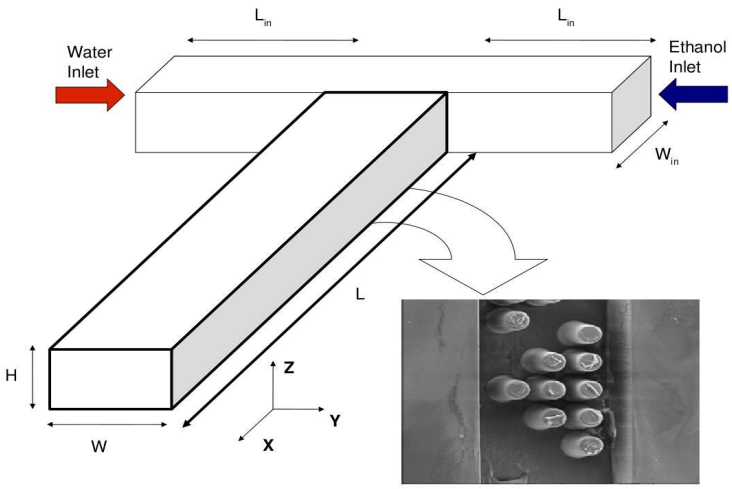

Figure 3: T-sensor geometry with obstacle layouts. The photographic image from[1] refers to part of one of the obstacle layouts considered in the experiments.

Like in the previous case $\psi^j = \rho^j$. Once ψ and the coupling matrix elements are fixed, the diffusivity is determined by measuring the decay of a concentration wave like what was done in[5,15] . The density and viscosity ratios match those of real fluids. In order to get the desired Peclet number of 200, the coupling matrix for this case is given by $\mathcal{G}_{11} = \mathcal{G}_{22} = 0$ and $\mathcal{G}_{12} = \mathcal{G}_{21} = 1.1$. The boundary conditions were Bounce-Back[2] on all obstacle surfaces and channel walls, Zou-He[8] scheme for inlet sections and extrapolation

scheme for the outflow section. In order to evaluate the gradient in equation (15) a "ghost" layer of nodes is placed immediately outside the outflow section: i and j are the indexes on x and y directions, the abscissas of a ghost node, outflow section node and inside node at constant j will be indicated by i, i_o and i_{o-1} respectively. The density on each node i_{o-1} is therefore extrapolated according to $\rho_i = \frac{4}{3}\rho_o - \frac{1}{3}\rho_{i-1}$.

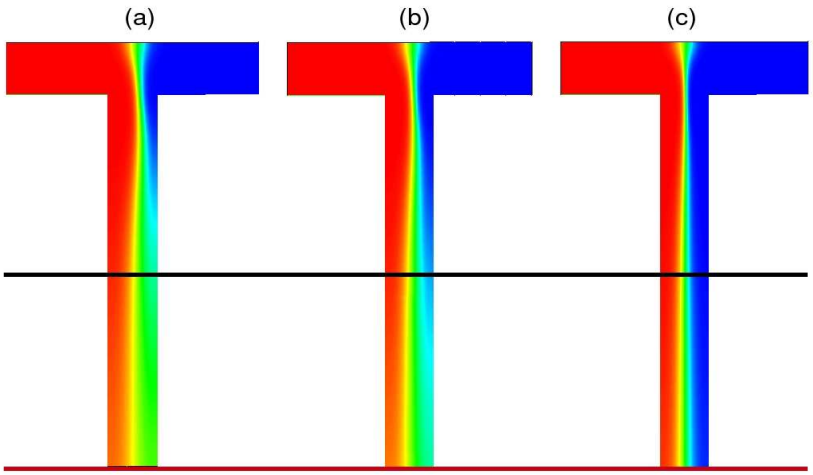

Figure 4: Fluid 1 concentration contours at different U: (a) 0.1, (b) 0.11, (c) 0.5.

The first test intends to evaluate the dependence of the mixer efficiency on the flow rate. No obstacles are considered here. figure 4 illustrates the effect of increasing fluid 1 (water) inflow speed U from 0.1 to 0.5 by showing fluid 1 (water) concentration contours. Both fluids have the same flow rate, so the inlet velocity of fluid 2 (ethanol) is adjusted accordingly. The concentration profiles for fluid 1 in the middle and at the outflow sections of the main channel (indicated with a red and a black line in figure 4) can be seen in figure 5 a and b. Slow flows do not need any obstacle to exhibit a high degree of mixing.

3.1 CONFIGURATIONS WITH CIRCULAR OBSTACLES

The different obstacle layouts adopted in[1] are listed in Table 2 and sketched in figure 6. Some configurations (indicated here and in the following as "C") are *included* in others with bigger number of obstacles, and therefore are represented in red. The channel is 1.2mm and 800 grid nodes long respectively in[1] and in the present study. The resulting lattice space Δx is therefore $1.5\mu m$, except for configuration 8, where the channel is 2.0mm long and 1000 nodes where used, for a $\Delta x = 2\mu m$. Table 3 compares the most relevant geometrical quantities indicated in figures 3 and 6 between LB simulations and[1] .

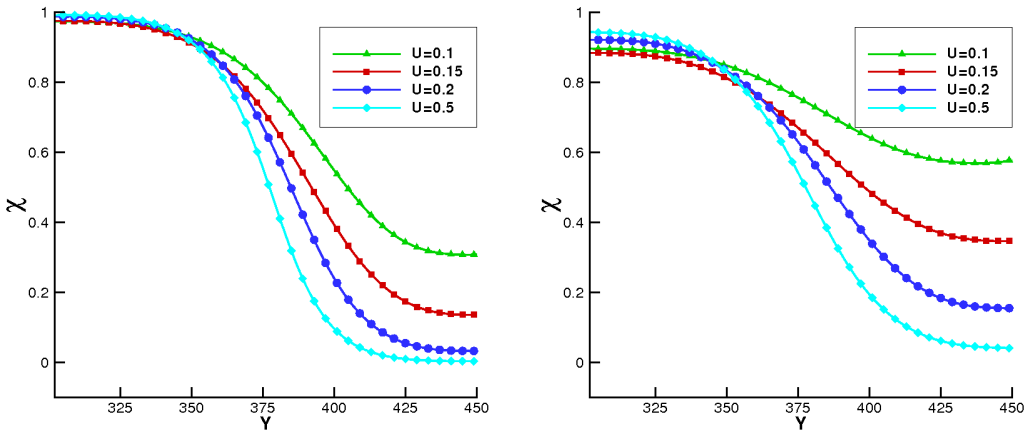

Figure 5: Concentration profiles for fluid 1 (water) at main channel mid- (a) and outflow sections (b).

Configuration number	1	2	3	4	5	6	7	8
Number of obstacles	0	1	1	2	3	9	9	18

Table 2: Different configurations tested in[1] and in the present study.

In what follows the inlet velocity of water is fixed to 0.5. Figure s 7-11 illustrate the performance of the different configurations. The obstacles brake the symmetry of parabolic velocity profile (here with a small discontinuity because of the small viscosity difference between the 2 fluids) giving diffusion more time to act. This is evident in figure 11 where the streamlines and velocity vectors are shown for configurations 4 and 8. The efficiencies are listed in Table 4: it is important to notice that it is not sufficient simply to place more obstacles to increase the mixing efficiency; the layout makes the difference. That is evident when comparing configurations 2 and 3: they are both characterized by one obstacle only, but the latter has it tangent to the middle of the channel. The better configurations are those which possess consecutive obstacles, or group of obstacles that induce migration in opposite directions. C8 proves to be the most efficient configuration, because it forces the fluid to migrate laterally more than any other configuration tested. Table 4 also reports the corresponding efficiencies computed in[1] , evidencing a close agreement with the performance of a commercial code. The only exception was configuration C3, which was found to be less efficient than C2, while in[1] it achieves twice the efficiency of C2. This discrepancy is probably due to a different vertical position of the obstacle in this study with respect to what is simulated in[1] , as confirmed by the very close match for the other seven configurations.

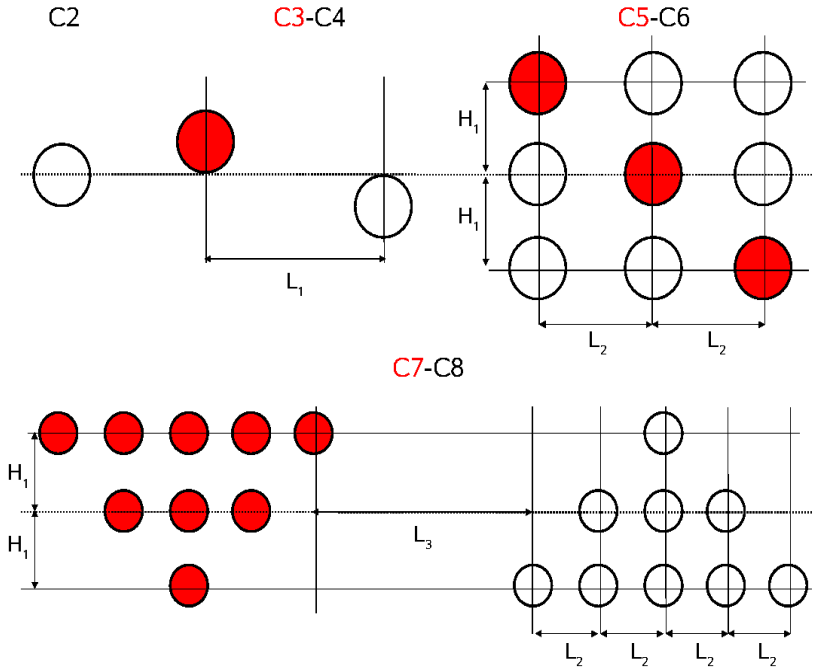

Figure 6: Geometry of the different configurations tested.

	L	H	W	W_{in}	L_{in}	D_{obst}	L_1	L_2	L_3	H_1
Wang[1](μm)	1200 (2000)	100	300	200	-	60	-	100	300	90
LU	800 (1000)	-	150	100	300	40 (30)	100	50	150	45

Table 3: Micromixer geometrical parameters in[1] expressed in μm and in the present study expressed in lattice units; the values in parentheses are related to configuration 8.

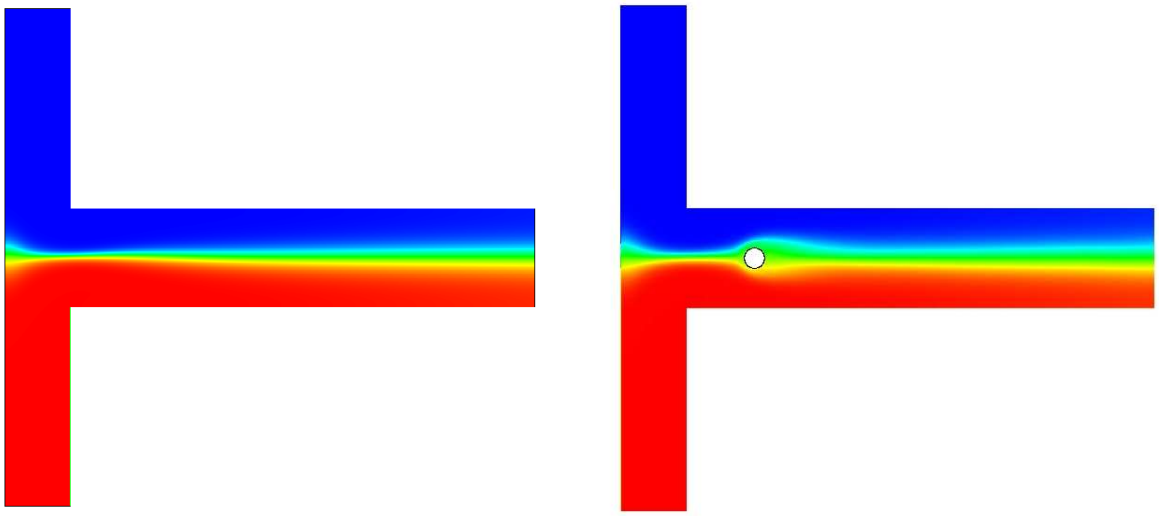

(a) C1 (b) C2

Figure 7: LB simulation of T-micromixer for configurations 1 and 2 as proposed in[1] .

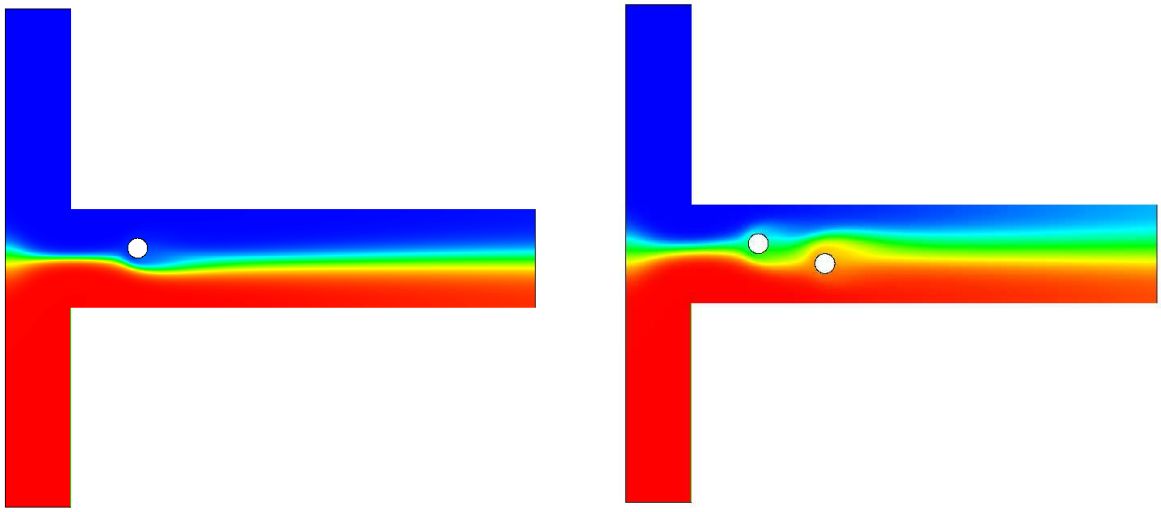

(a) C3 (b) C4

Figure 8: LB simulation of T-micromixer for configurations 3 and 4 as proposed in[1] .

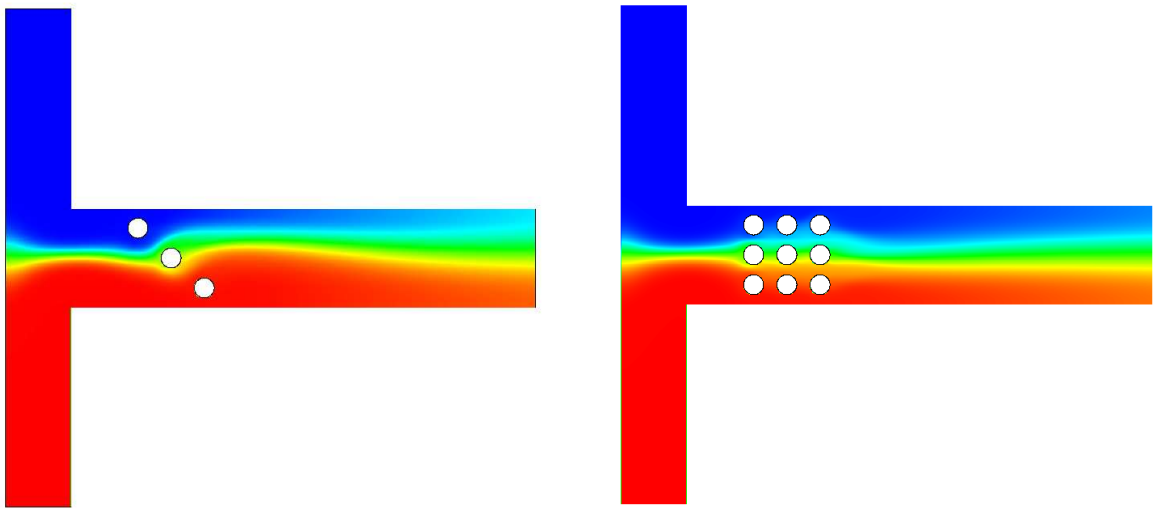

(a) C5 (b) C6

Figure 9: LB simulation of T-micromixer for configurations 5 and 6 as proposed in[1] .

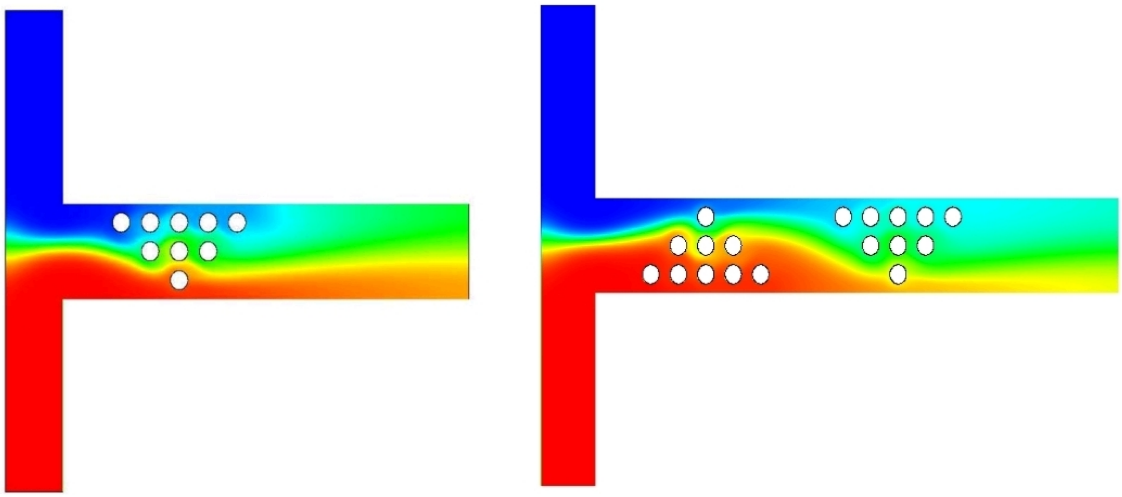

Figure 10: LB simulation of T-micromixer for configurations 5 and 6 as proposed in[1] .

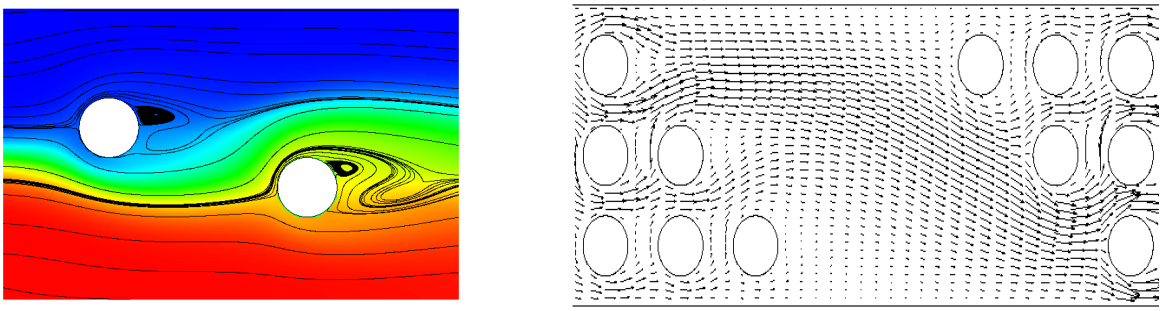

(a) C4 (b) C8

Figure 11: Particular of streamlines (a) and velocity vectors (b)for C4 and C8.

	Configuration							
Efficiency (%)	1	2	3	4	5	6	7	8
Wang[1]	18.0	21.0	42.0	44.0	46.0	32.0	53.0	62.0
LB	17.2	22.0	31.5	43.8	46.2	31.4	51.3	60.8

Table 4: Comparison between the mixing efficiency in[1] and those computed in the present study with LB for all the different configurations.

4 CONFIGURATIONS WITH RECTANGULAR OBSTACLES

Once demonstrated that the presence of obstacles stir the flow in the transverse direction promoting mixing it is possible to test the device with obstacles differently shaped. In this section the parameters are the same of configurations 1-7, but there are only two rectangular obstacles. Three tests were conducted, in order to evaluate the influence on mixing of three different geometrical parameters, namely the *degree of blockage*, the *offset* and the *gap* between obstacles. These parameters are defined as in[16] and have been sketched in figure 12.

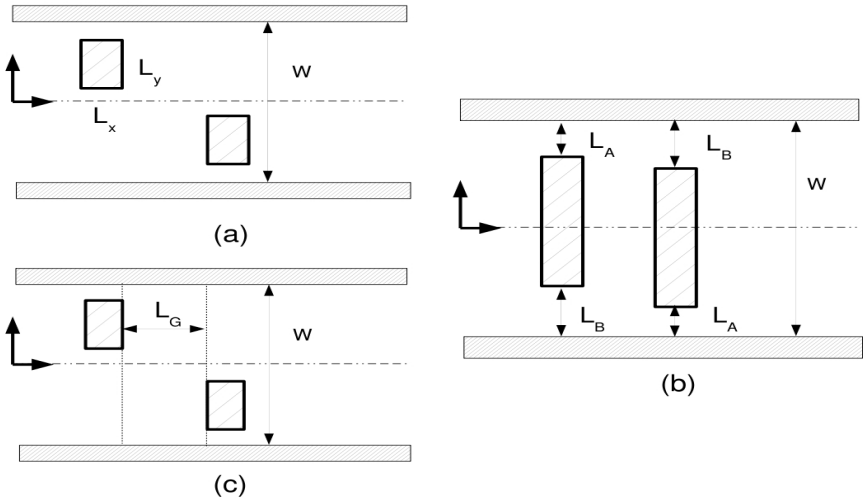

Figure 12: Sketch of the different tests conducted with rectangular obstacles: a) Blockage; b) Offset; c) Gap.

The degree of blockage is defined as L_y/W. Observing Figure 13 it is possible to notice how increasing this parameter improves ε_{mix} till a certain amount, when the fraction of distorted flow dropped.

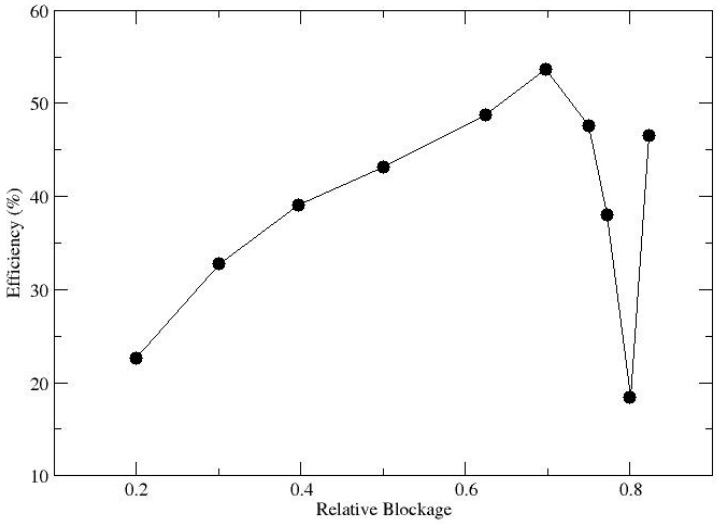

Figure 13: Sketch of the different tests conducted with rectangular obstacles: a) Blockage; b) Offset; c) Gap.

The offset measures the relative position of the obstacles respect to channel walls: it is defined by L_A/L_B. As it appears clearly in Figure 12, when the obstacles touch the

channel walls the offset is null, while when the obstacles are symmetrically placed with respect to the centre of the channel this parameter is one.

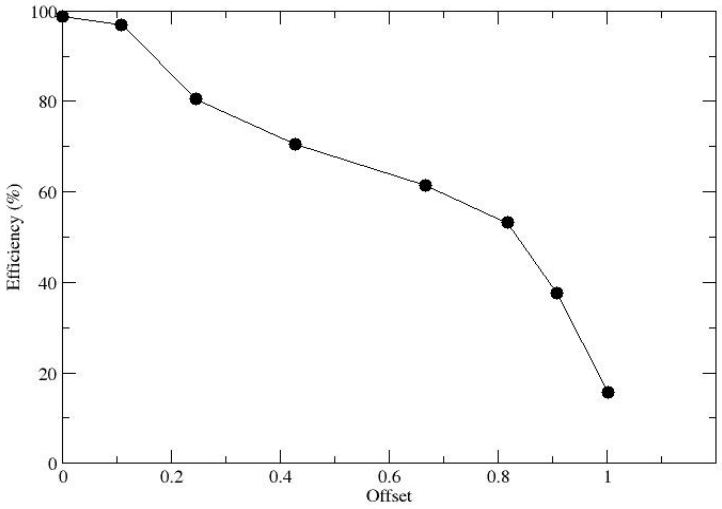

Figure 14: Sketch of the different tests conducted with rectangular obstacles: a) Blockage; b) Offset; c) Gap.

In the first case the efficiency reaches its maximum (serpentine channel), while ε_{mix} decreases once the obstacles approach the centre of the channel. Figure 14 summarizes these results. Finally the relative gap between obstacles was defined as L_G/W. As can be seen in figure 15 the performance improved as the gap was increased.

5 CONCLUSIONS

- Passive micromixers are the simplest devices to promote mixing in Lab-On-a-Chip devices. Unfortunately diffusion is not an effective mean to achieve a high mixing degree in short microchannel lengths.
- The introduction of obstacles can significantly improve the performance of a passive mixer by inducing some lateral convective flow.
- The Lattice Boltzmann method was shown to provide results comparable with those reported in[1] using a commercial code.
- The results show that it is not necessary to place a great number of obstacles in the main channel of the T-sensor. High mixing efficiencies can be in fact achieved by simply placing few asymmetric obstacles in a "suitable" way.
- The tests conducted with rectangular obstacles provided guidelines for a "suitable" placement: mixing efficiency is significantly lifted by increasing the obstacle gap and by decreasing the offset.
- The results presented, together with the parallel nature of LB algorithm are en-

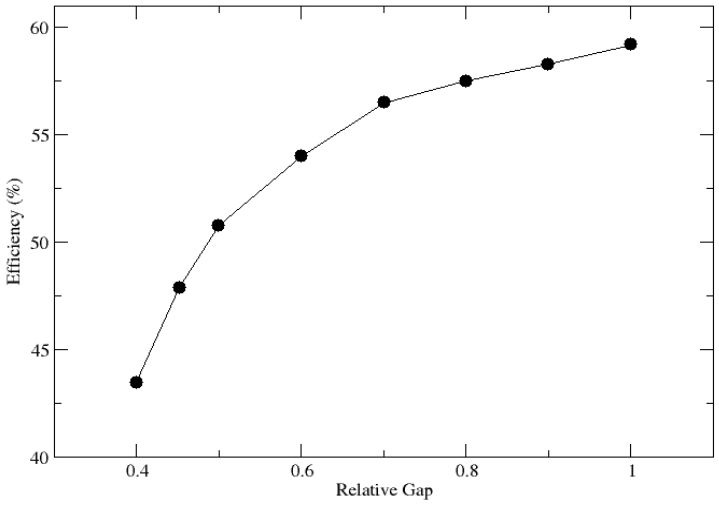

Figure 15: Sketch of the different tests conducted with rectangular obstacles: a) Blockage; b) Offset; c) Gap.

couraging for an analogous three-dimensional study, which in fact will be the subject of future work.

REFERENCES

[1] H. Wang and P. Iovenitti and E. Harvey and S. Masood, Optimizing the layout of obstacles for enhanced mixing in microchannels, *Smart Mat. Struct.*, **11**, 662–667 (2002).

[2] S. Chen and G. Doolen, Lattice Boltzmann model for fluid dynamics, *Annu. Rev. Fluid Mech.*, **30**, 329–364 (1998).

[3] Y. H. Quian, D. d'Humieres and P. Lallemand, Lattice BGK models for the Navier-Stokes equation, *Europhys. Lett.*, **17**, 479–484 (1992).

[4] X.W. Shan and H.D. Chen, Lattice Boltzmann model for simulating flows with multiple phases and components, *Phys. Rev. E*, **47**, 1815 (1993).

[5] X.W. Shan and H.D. Chen, Simulation of non-ideal gases and liquid-gas phase transition by the Lattice Boltzmann equation,*Phys. Rev. E*, **49**, 2941–2948 (1994).

[6] F. Wolf, L. O. E. dos Santos and P. Philippi, Fluid interfaces in phase transition problems: Lattice Boltzmann Method, In proceedings of the *18th International Congress of Mechanical Engineering*, COBEM (2005).

[7] M. Sbragaglia, R. Benzi, L. Biferale, S. Succi, K. Sugiyama and F. Toschi, Generalized lattice Boltzmann method with multirange pseudopotential, *Phys. Rev. E*, **75** (2007).

[8] Q. Zou and X. He, On pressure and velocity flow boundary conditions and bounceback for the lattice Boltzmann BGK model, *Phys. Fluids*, **9**, 1591–1598 (1997).

[9] J. Chin and P. Coveney, Lattice Boltzmann study of spinodal decomposition in two dimensions, *Phys. Rev. E*, **66** (2002).

[10] A. Einstein, On the motion of small particles suspended in liquids, *Ann. Phys. Lpz.*, **17**, 549–560 (1905).

[11] E. M. Purcell, Life at low Reynolds number, *Am. J. Phys.*, **45**, 3–11 (1977).

[12] V. Hessel, H. Löwe and F. Schönfeld, Micromixers-a review on passive and active mixing principle, *Chem. Eng. Sci.*, **60**, 2478–2501 (2005).

[13] D. Gobby, P. Angeli and A. Gavriilidis, Mixing characteristics on T-type microfluidic mixers, *J. Micromech. Microeng.*, **11**, 126–132 (2001).

[14] N. L. Jeon, S. K. W. Dertinger, D. T. Chiu, I. S. Choi, A. D. Strook and G. M. Whitesides, Generation of solution and surface gradients using microfluidic systems,*Langmuir*, **16**, 8311–8316 (2000).

[15] E. G. Flekkøy, Lattice BGK models for miscible fluids, *Phys. Rev. E*, **47**, 4247–4258 (1993).

[16] H. Wang, P. Iovenitti, E. Harvey, and S. Masood, Mixing of liquids using obstacles in microchannels, In proceedings of *BioMEMS and Smart Nanostructures*, SPIE **4590**, 204-212 (2001).